Defect structure analysis in single crystal substrates using XRTmicron

Katsuhiko Inaba*

1. Introduction

For more than 50 years, X-ray topography (XRT) has been an indispensable industrial and research tool for crystal growth of functional materials, since crystalline defects, such as dislocations, stacking faults, etc., can be detected with this technique non-destructively. Industrial demand for almost dislocation-free Si has greatly contributed to this technique, providing important insights for the improvement of crystal quality.

These days, various functional bulk single crystals other than Si have been grown and industrial application of these crystals have been explored. X-ray topography is also employed to investigate growth conditions and correlations between physical properties and crystalline qualities of these crystals.

Even for Si wafers that are originally dislocation-free, there is a possibility that strains and/or defects will be introduced during steps in device fabrication processes; thus, there arises a need for non-destructive characterization without changing the device structure fabricated on the Si wafers. X-ray topography is, therefore, used not only for characterization of slices of ingots or bare wafers, but also for the inspection of processed wafers.

In this article, important features and functions equipped in Rigaku's latest X-ray topograph apparatus, XRTmicron™ [(1)–(3)] are reviewed briefly and application data from this apparatus related to modern functional crystals will be introduced.

2. Features of XRTmicron

Some important features and functions equipped in XRTmicron are listed below[(2)].

- Dual-wavelength high-brilliance microfocus X-ray source (including automatic target changing function)
- Employs a multilayer X-ray mirror optic system
- Automatic switching between transmission and reflection geometries
- Employs high-sensitivity, high-resolution X-ray digital camera
- "3D section topography" measurement

In this section, features and functions of unique and powerful 3D section topography measurements will be discussed, with which three-dimensional defect configurations in the interior of a crystal can be observed nondestructively.

The geometry for conventional section topograph measurements is shown in Fig. 1. By introducing a narrow slit between the sample (wafer) and the incident optic system, a narrow line-shaped incident beam strikes a sample. The depth of a defect in the interior of the sample can be determined by correlating the thickness of the sample and the position of the defect image on a 2D detector.

By simultaneously employing a high-brilliance microfocus X-ray source and a multilayer X-ray mirror optic system, it is possible to acquire a high-definition image in an extremely short exposure time (for example, 10 seconds) with laboratory apparatus. Additionally, development processes, which were required for conventional recording media such as X-ray films or imaging plates, used in older XRT systems, are no longer necessary because an X-ray camera that records images as digital data is employed in the XRTmicron system. As a consequence, the iterative processes of step shifting a sample and image acquisition are enabled successively, as is continuous image collection without stopping the apparatus. Multiple image collection can be initiated by a simple input of parameters, such as exposure time, sample shift step size, total length of

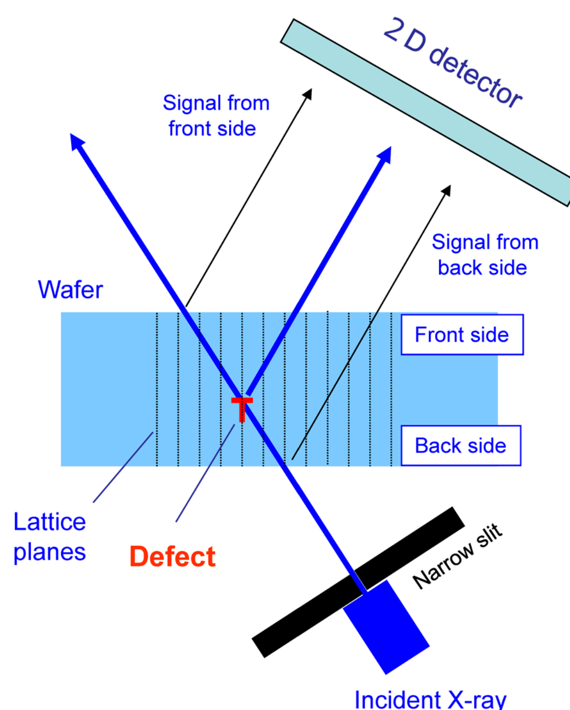

Fig. 1. Geometry for section topography.

* X-ray Research Laboratory, Rigaku Corporation.

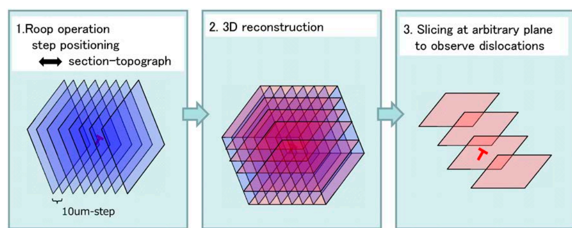

Fig. 2. Procedure of data processing of 3D section topography.

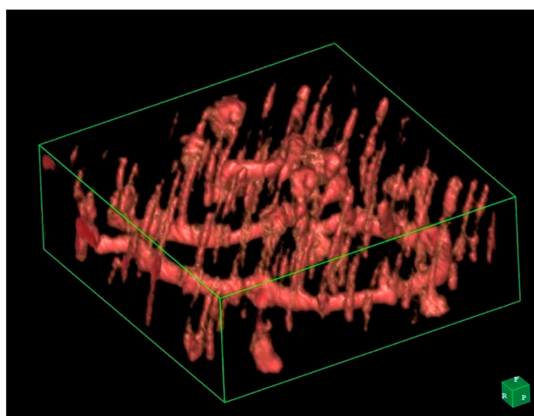

Fig. 3. Example of 3D section XRT image (4H-SiC).

sample shifting, etc., into the XRTmicron operation software. We call this process of 3-dimensionally collecting images of the interior of a single crystal sample a "3D section topography measurement". Multiple image data obtained are merged into a united file after measurement, and a 3D reconstruction process is performed on this combined file (Fig. 2.). Details of defect configuration can also be observed at arbitrary cross-sections of the 3D-reconstructed file. An example of 3D section topography data is shown in Fig. 3. The sample is a 4H-SiC wafer[(1), (3)]. The size of cuboid image is 1.5 mm × 1.5 mm × 0.3 mm (= wafer thickness), clipped from the 3D reconstructed data. The shortest dimension of the object is perpendicular to the sample surface. Short straight segments running along the vertical line of the figure are treading screw dislocations (TSDs) or treading edge dislocations (TEDs), and the swirling long line is the basal plane dislocation (BPD), which runs in the (0001) plane of 4H-SiC.

3. Characterization of Dislocations by XRT

XRT is a technique to observe defects in a sample by recording diffracted signals in a 2D recording medium where the differences of signals from perfectly crystalline areas and from defected areas containing lattice distortion are essential. This fact leads to a unique and useful feature of XRT: this technique can determine the Burgers vector (vector of local atomic displacement) of a dislocation, which differentiates this technique from other analytical techniques that don't use diffraction phenomena. The criteria to determine the Burgers vector can be simply explained as follows. The contrast

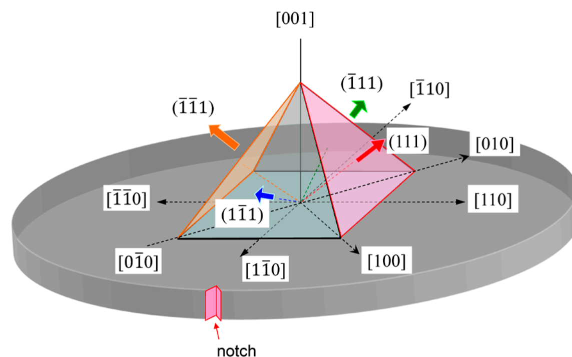

Fig. 4. Crystallographic axes and {111} slip planes of Si(001) wafer.

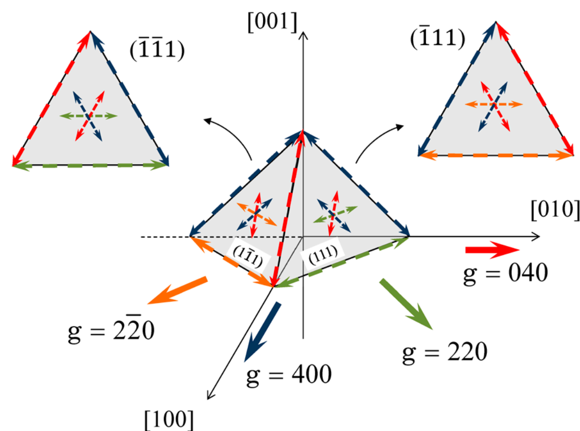

Fig. 5. Schematic illustration of the relationship of {111} slip planes, Burgers vectors for Si(001) and diffraction vectors.

of the differences of signals from perfectly crystalline areas and from defected areas will disappear when the diffraction vector ($\boldsymbol{g}$) of the image and the Burgers vector ($\boldsymbol{b}$) are perpendicular to each other; i.e., the inner product of these vectors equals zero ($\boldsymbol{g}\cdot\boldsymbol{b}=\mathbf{0}$)[(4)–(6)]. This kind of analysis is known as $\boldsymbol{g}\cdot\boldsymbol{b}$ analysis.

Let us examine a case of a Si (001) wafer. Si is known to have a diamond type crystal structure. The major slip line for this type of crystal structure is $1/2\langle 110\rangle$ {111}, i.e., dislocations slip on {111} with a Burgers vector of $1/2\langle 110\rangle$. All {111} slip planes intersect with the (001) surface plane at an angle of 54.7°. By taking into account the four-fold symmetry of Si (001), all these {111} slip planes can be expressed as triangular pyramidal planes of an octahedron as shown in Fig. 4, where the upper half of the octahedron is shown. Edges of the octahedron, thus the outlining segments of the triangular faces, are aligned to be parallel to Burgers vector (Fig. 5.). There are 12 edges in total. Four of them run parallel to the (001) sample surface, another four intersect with the (001) sample surface, and the final four exist beneath the (001) plane. The last group of four edges is not shown in Fig. 5.

Next, dislocation analysis for the slip dislocations in a Si (001) wafer is discussed. Slip dislocations are observed in Si wafers after thermal annealing. The

220 and 400 reflections are both often employed in transmission geometry to detect slip dislocations in a Si (001) wafer, since both diffraction vectors run parallel to the sample surface. Displacement caused by slips through thermal stress is also expected to be parallel to the sample surface, i.e., directed along $\pm[110]$ (shown as orange dashed lines in Fig. 5.) or along $\pm[1\bar{1}0]$ (shown as green dashed lines in Fig. 5.). The diffraction vector for the 220 reflection (shown as a green solid line) is found to be perpendicular to the $\pm[1\bar{1}0]$ direction (shown as green dashed lines). This leads to the situation where the contrast for images of dislocations with $\boldsymbol{b}//\pm[1\bar{1}0]$ should disappear. Using the same logic, dislocations with $\boldsymbol{b}//\pm[110]$ should disappear in images for $2\bar{2}0$ reflection, whose diffraction vector is shown as an orange solid line. However, when XRT images are taken for the 400 reflection, contrast in these images for the dislocations mentioned above will not disappear, because the diffraction vector for 400 reflection (blue solid line) does not intersect at a right angle either with the $\pm[110]$ directions or the $\pm[1\bar{1}0]$ directions. This fact means that the 400 reflection or the 040 reflection, whose diffraction vector is shown as a solid red line, can be conveniently employed for the purpose of recording all dislocations whose Burgers vectors are parallel to the sample surface, though determination of their Burgers vectors is not accomplished with these images. You may notice that employment of the 220 reflection or the $2\bar{2}0$ reflection for X-ray topograph measurements of a Si (001) sample will result in the situation where determining Burgers vectors for dislocations either with $\boldsymbol{b}//\pm[110]$ or with $\boldsymbol{b}//\pm[1\bar{1}0]$ is possible but recording images of all of these dislocations in a single XRT image cannot be satisfied.

Burgers vectors, which intersect with the surface plane for Si (001), are also shown in Fig. 5. In this figure, diffraction vectors are shown in colored solid lines and Burgers vectors are shown in colored dashed lines. Solid lines and dashed lines of the same color intersect orthogonally with each other.

4. Application Examples of Modern Functional Crystals

4.1. Sapphire substrates

A major application of sapphire single crystal substrates in industry is their use as substrates for the growth of GaN epitaxial films for blue LEDs. Currently *c*-plane sapphire substrates are widely adopted for this application[7]. It may be of interest in the field of pure material sciences and also in the field of industrial applications whether defects originally existing in sapphire wafers will not be affected during/after the GaN growth processes performed at a severely high temperature of around 1000°C. It is not easy to characterize defects in the interior of sapphire substrates after GaN growth in the production of LEDs because the front sides of the sapphire wafers are covered with thick GaN layers and the surfaces of their back sides are normally not flat nor in mirror-polished condition.

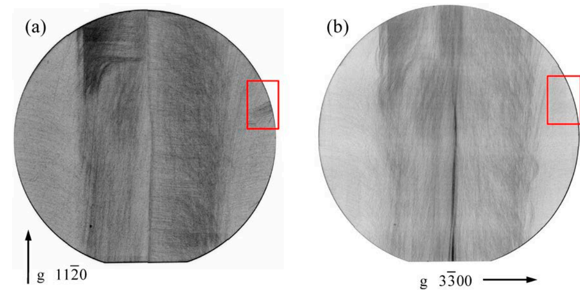

Fig. 6. A transmission XRT images of sapphire with GaN epitaxial film.
(a) $11\bar{2}0$ reflection, (b) $3\bar{3}00$ reflection.

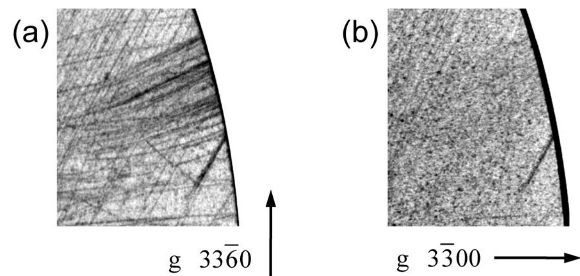

Fig. 7. Magnified views of areas marked with red lines in Fig. 6.
(a) $33\bar{6}0$ reflection, (b) $3\bar{3}00$ reflection.

This prevents optical characterization techniques from accessing the interior of the sapphire substrates, but XRT can access this region nondestructively.

The crystal structure of sapphire is known as the corundum (α-Al_2O_3) type, which is in the rhombohedral (or trigonal) lattice system with three-fold symmetry. The unit cell of this structure can be expressed using either a rhombohedral lattice or a hexagonal lattice. The latter hexagonal setting is more common and is the one used in this article. The slip systems for the corundum structures are reported in Ref. 8–10. The most common and major slip system, $1/3\langle 11\bar{2}0\rangle(0001)$, is known as the "basal slip system," where the slip plane is the basal (0001) plane, and the Burgers vector of the dislocations is either one of $1/3\langle 11\bar{2}0\rangle$. This slip system is predominant especially at high temperature. At moderate or low temperatures, slip systems other than the basal slip system are also active. One of them is the "prismatic slip system," $\langle 1\bar{1}00\rangle\{11\bar{2}0\}$, where the slip plane is the prismatic $\{11\bar{2}0\}$ plane, and the Burgers vector of the dislocations is $\langle 1\bar{1}00\rangle$. There are reports of another less commonly observed candidate known as the "pyramidal slip system," slipping on the $\{1\bar{1}0L\}$ or $\{11\bar{2}L\}$ planes.

A transmission topograph image of a 2-inch sapphire (0001) wafer with 2 μm-thick GaN epilayer is shown in Fig. 6. In this figure, the image contrast was set so that pixels recording strong signals are shown in dark color. This means that dislocations and the wafer edge are shown in black. Magnified views of areas marked with red lines in Fig. 6(a) and (b) are shown in Fig. 7(a) and (b), respectively. Fig. 7(a) was taken for the $33\bar{6}0$

reflection. Dislocations running close to the horizontal direction are clearly visible in Fig. 7(a), while these dislocations are out of contrast in Fig. 7(b). This indicates that the Burgers vector for these dislocations is perpendicular to the diffraction vector ($\boldsymbol{g}=3\bar{3}00$) for the image in Fig. 7(b). In other words, we can only say that the Burgers vector is laying in ($1\bar{1}00$), but details of its slip system cannot be identified. Another fact that is deduced from a comparison of Fig. 7(a) and (b) is that lines of the dislocations that are out of contrast in Fig. 7(b) are almost parallel to the [$1\bar{1}00$] direction, which is perpendicular to their Burgers vector, thus these dislocations must be deemed edge-type dislocations. If we recall the fact that the major slip system of sapphire crystals is $1/3\langle 11\bar{2}0\rangle(0001)$, it is a safe assumption that the dislocations out of contrast in Fig. 7(b) are the ones in the $1/3[11\bar{2}0](0001)$ slip system .

Figure 8(a) and (b) show data from a transmission 3D section X-ray topography for this sapphire substrate [11]. Complex defect configuration in this figure is shown in negative contrast, where white denotes stronger intensities. Some dislocations clearly observed in Fig. 8(a) for the $33\bar{6}0$ reflection are missing in Fig. 8(b) for the $6\bar{6}00$ reflection. These are the same edge dislocations discussed in the previous paragraph, with $\boldsymbol{b}=1/3[11\bar{2}0]$ slipping on (0001). Almost all other dislocations in Fig. 8(a) and (b) seem to run in (0001) and they are not threading dislocations outcropping to the interface with the GaN epitaxial layer. This finding may suggest that most dislocations occurring in sapphire substrates will not easily outcrop to interfaces for GaN growth when the (0001) plane of sapphire substrate is employed.

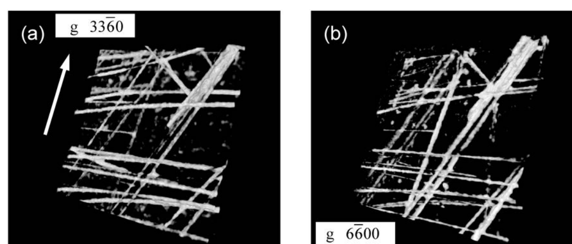

Fig. 8. 3D section XRT image for the sapphire substrate. (a) $33\bar{6}0$ reflection, (b) $6\bar{6}00$ reflection

The 3D section XRT images shown in Fig. 8 were constructed using data from a 2.5 mm square in which damaged layers of sapphire substrate—both on its front side (GaN layer side) and on its back side (without mirror polishing)—were removed from the original data. This kind of data treatment is possible for 3D section XRT, enabling data analysis with clear images of the interior of substrates by suppressing the contribution of damaged surface regions.

Sapphire substrates with various surface planes other than *c*-plane are commercially available. For example, *m*-plane sapphire substrates are used for research to grow nonpolar GaN epitaxial films, *r*-plane substrates for SOI (silicon on insulator) structure, *a*-plane substrates for applications such as protective window materials of cellar phones, etc. Surface planes of all these sapphire substrates intersect with the *c*-plane, thus it is inevitable that dislocations of major slip systems stored in sapphire substrates may outcrop to their surfaces. Various growth techniques of sapphire ingots have been reported, such as the Kyropoulos method, the EFG (Edge-defined Film-fed Growth) method, the CZ (Czochralski) method, the VHGF (Vertical Horizontal Gradient Freeze) method, the HEM (Heat Exchange method), etc. It is of great interest whether there are variations of defect configurations or of defect nature.

Figure 9 shows XRT images for an *m*-plane bare sapphire wafer. This wafer was of 2 inches in diameter and 350 μm thick. Surface treatment for this wafer for both the front and back sides was finished with lapping treatment before mirror polishing. The image in Fig. 9(a) was obtained with Cu Kα_1 radiation in reflection geometry ($4\bar{2}\bar{2}0$ refection). The *c*-axis of the sapphire crystal is aligned to be horizontal in the figure. The effective penetration depth in this diffraction condition, where diffracted signals will be weakened by 1/e due to the mass absorption effect, is calculated to be 12 μm.

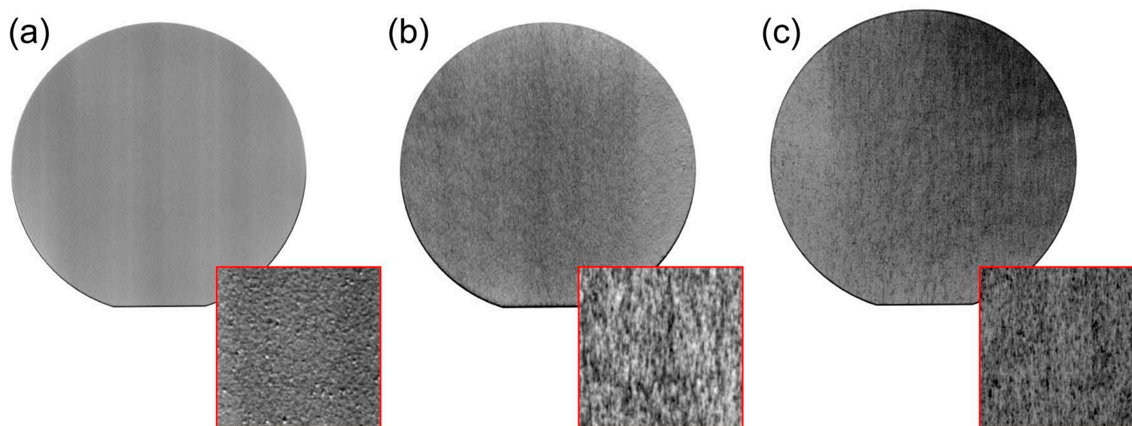

Fig. 9. XRT images of an *m*-plane sapphire substrate with rough surface.
(a) Reflection geometry with Cu radiation ($4\bar{2}\bar{2}0$ reflection), (b) Reflection geometry with Mo radiation ($10\bar{5}\bar{5}0$ reflection), (c) Transmission geometry with Mo radiation ($33\bar{6}0$ reflection). (Inserts are the magnified images of 5 mm-square area for each images)

This means that the image recorded in Fig. 9(a) mostly contains contributions from the surface damaged layer rather than from the interior of the sapphire substrate. The inset figure in the lower right corner in Fig. 9(a) is the magnified image of the central 5 mm square region. In this inset figure, dislocations in the interior of the sapphire body cannot be observed. The image in Fig. 9(b) was also obtained in reflection geometry, but recorded using Mo Kα_1 radiation ($10\bar{5}\bar{5}0$ refection). The effective penetration depth in this diffraction condition is calculated to be 180 μm. This value corresponds to half of the sample thickness, thus it is expected that the major contribution for this image may be the interior of sapphire substrate. The magnified image of the 5 mm square central area is shown as the inset figure at the lower right corner in Fig. 9(b). Lines of defects running in the vertical direction, thus parallel to *c*-plane of the sapphire crystal, can be observed as short segments whose configuration relative to the sapphire lattice is consistent with the major slip system of $1/3\langle 11\bar{2}0\rangle$ (0001). Additionally, an XRT image with transmission geometry with Mo Kα_1 radiation was also obtained ($3\bar{3}60$ refection). It is expected that lines of defects (dislocations) will be detected as vertical short segments (or dots) in this diffraction condition for dislocations of the major slip system of the sapphire crystal. The result is shown in Fig. 9(c), where dislocations are observed as short segments running vertically, as expected. Since the transmitting power of Mo Kα_1 radiation against materials is larger than that of Cu Kα_1 radiation, you can probe deeper into the interior of a sample in reflection geometry with Mo Kα_1 radiation than with Cu Kα_1 radiation. This is effective for cases such as characterizing wafers without polished surfaces as discussed previously, or to inspect processed wafers over which functional films are grown and wafers are masked by those film. Employing Mo Kα_1 radiation for reflection geometry may be useful for accessing to interiors of very thick samples, such as ingots, or for samples coated with thick and dense substances, where measurement with transmission geometries is not applicable. Conversely, when the vicinity of the surface of polished wafers is the region of interest, it is better to employ Cu Kα_1 radiation.

The standard XRTmicron system is equipped with a dual-wavelength X-ray source (Cu and Mo). Switching the X-ray source can be performed within several minutes under software control without breaking the vacuum system. Switching between transmission and reflection geometry can also be performed automatically by the software.

4.2. SAM ($ScAlMgO_4$) substrate

$ScAlMgO_4$ is a substrate developed by Bell Laboratory in the USA in the 1990s, intended for use as a substrate for GaN growth for blue LEDs. It used to be called "SCAM." Much attention was focused on this material due to the small lattice mismatch and small difference in thermal expansion coefficients between it and GaN. However, this material was not widely supplied on a commercial basis because of the difficulties in bulk crystal growth. Its crystal structure is known as the $YbFe_2O_4$-type structure, in space group $R\bar{3}m$(#166). It is constructed by stacking layers of a rock salt-type structure and a zinc blende-type structure, with the cleavage plane of (0001). A unit cell of this structure can be expressed as a hexagonal cell with lattice constants $\boldsymbol{a} = 0.3256$ nm and $\boldsymbol{c} = 2.516$ nm[12]. Recently, it was reported that high-quality SAM substrates 2-inches in size were grown by the CZ method by Fukuda Crystal Laboratory in Japan[13]–[15].

A transmission XRT image for a 2-inch (0001) SAM substrate around 0.5 mm thick is shown in Fig. 10(a) for the $22\bar{4}0$ reflection. Concentric triangular patterns with rounded corners observed in the image are assumed to be correlated with striation patterns originating from local fluctuations in the composition of constituent atoms, following the crystallographic symmetry of this crystal. Since these concentric triangular patterns are observed over the whole area of the sample, it is expected that an extremely low number of dislocations is contained in this SAM substrate. High-resolution rocking curve analysis was performed for this sample using the SmartLab multipurpose XRD system. An extremely narrow rocking curve profile with FWHM (Full Width at Half Maxima) value of 0.002° (7.2

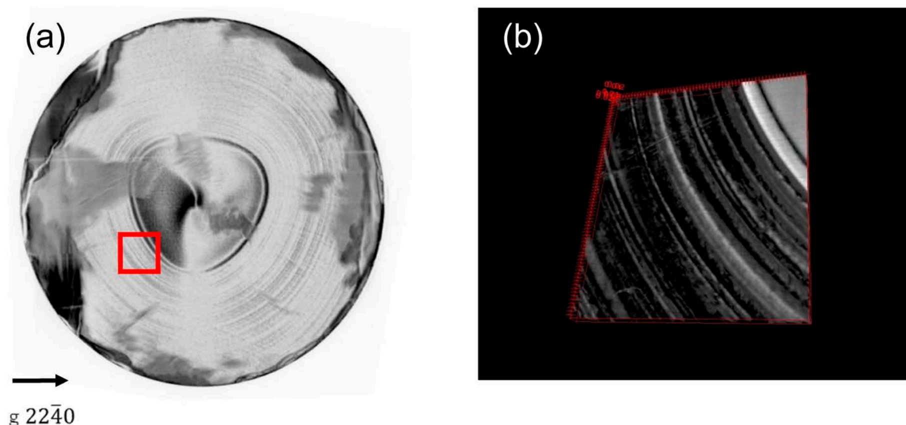

Fig. 10. (a) A transmission XRT image for SAM substrate, (b) a 3D section XRT image.

arcsec) was obtained using a Ge 440 4-bounce incident beam conditioner for the 00018 reflection of SAM. This result is also a good indication of the high crystalline quality of the present sample. The resolution of this incident optic system is 0.0015°. A 3D section XRT data for the area of 6×7 mm marked by red lines in Fig. 10(a) is shown in Fig. 10(b). Striations can be seen as arcs in the figure. Only a few dislocations can be faintly detected as narrow straight lines running from the lower left to the upper right.

4.3. MgO substrate

A 3D section XRT data of commercially available MgO (001) substrate (10 mm×10 mm×0.5 mm) is shown in Fig. 11 (040 reflection). The image at the center of Fig. 11 is the cross-sectional image parallel to the sample surface (and also to MgO (001)) in the vicinity of the surface (30 μm below surface). Images of other planes orthogonal to the sample surface, i.e. parallel to MgO (100) and MgO (010), are shown at the right side and bottom side of Fig. 11, respectively. Sectioning positions for the latter two images are shown by the two red broken lines in the center image of Fig. 11. Figure 11 reveals that this crystal is composed of mm-sized grains with a slight misorientation to each other. Diffraction signals for grains at the right-bottom corner of the crystal are so weak because the degree of misorientation against the surrounding grains is so large that their diffraction conditions are not satisfied well. Grain boundaries in images at the right side and bottom side of Fig. 11 are shown in green broken lines. Scars (scratches), probably created during the lapping processes, can be seen in the area marked by blue circles in the center image of Fig. 11.

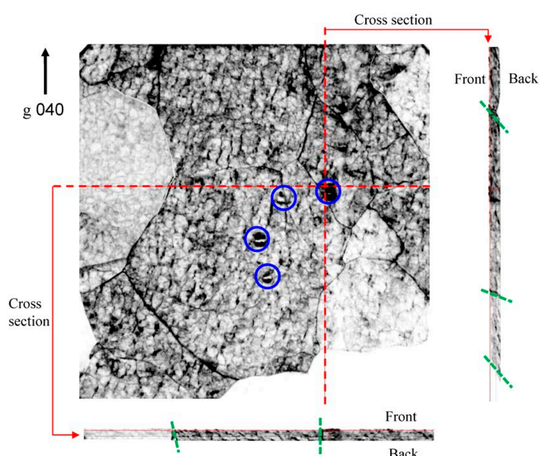

Fig. 11. A 3D section XRT image of MgO(001) substrate.

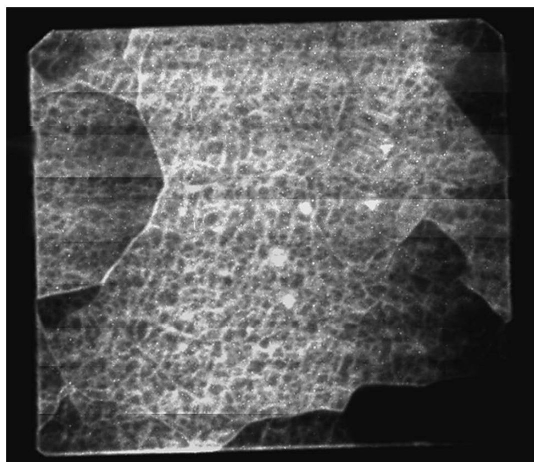

Fig. 12. A reflection XRT image of MgO substrate using SmartLab with XTOP camera.

A new function to record XRT images has been recently introduced to the SmartLab multipurpose XRD systems, enabled by installing an X-ray recording digital camera as an optional device to the system. An XRT image recorded with a SmartLab system equipped with XTOP camera for the MgO (001) sample described in the previous paragraph is shown in Fig. 12 (negative contrast). This image was recorded in reflection geometry with Cu Kα_1 radiation at an exposure time of 2 min. In this image, subgrain structures in the sample or defects in the interior of grains can be clearly observed. Though there are some limitations for XRT measurements by the SmartLab system, such as it being limited to reflection geometry, etc., X-ray topography with multipurpose XRD systems is currently available.

5. A Hot Topic with XRTmicron

Silicon carbide (SiC) is a modern functional single crystal material attracting great attention in industrial fields. Among various polytypes of SiC, 4H-SiC is a promising candidate as a wide bandgap semiconductor for electronic devices in power electronic applications. Improvement of device performance is greatly owed to the effort of reducing defect density in SiC crystals, and characterization of defects in SiC is getting more important these days. XRTmicron contributed to a research study discussing correlations of defect structures with the degradation process of *p-i-n* diodes with 4H-SiC(16). Automated dislocation evaluation software that analyzes digital topography images to count dislocations and identify their types is provided by Rigaku as an optional analysis software.

However, there are various types of defect characterization techniques besides XRT. Principles and features of major techniques to characterize crystalline defects are summarized in Table 1. Each has its own strong/weak points. Chemical etching has been a common technique for defect characterization of SiC for a long time. Recently, a high-throughput inspection system, SICA88(17), was introduced by Lasertec Corporation, Japan, that combines two characterization techniques such as the PL method and surface optical inspection. It has become widely employed for the purpose to defect analysis in SiC. A Tsukuba Power Electronics Constellation (TPEC)(18) project lead and organized by National Institute of Advanced Industrial Science and Technology (AIST) of Japan has announced the collaborative development of a new function in the

Table 1. Various characterization techniques of crystalline defects.

Methods	Principles/Features
XRT (XRTmicron)	– Burgers vector of dislocations can be determined, by changing diffraction conditions – Nondestructive, possible to analyze Boules or as-sliced wafers etc
Photoluminescence (PL) imaging	– Luminescence excited by laser light, shift of energy caused by defects – High-through put – Heating of samples by absorption of exciting light
Optical surface inspection	– Scanning optical microscopy using confocal DIC optic (Differential Interference Contrast) – Very sensitive to surface – Difficult in determining dislocation types
Mirror electron microscope[19][20]	– Observing electrons repulsed by surface electric field – Very sensitive to surface structure, – under vacuum condition – Difficult in determining dislocation types
Chemical etching	– Defected regions are selectively etched by etchant – Commonly used for a long time, relatively inexpensive – Destructive, safety measures to toxic etchant are required
Transmission electron microscopy (TEM)	– Burgers vector of dislocations can be determined, by changing Electron beam diffraction conditions – High spatial resolution but limited volume (area) of sample

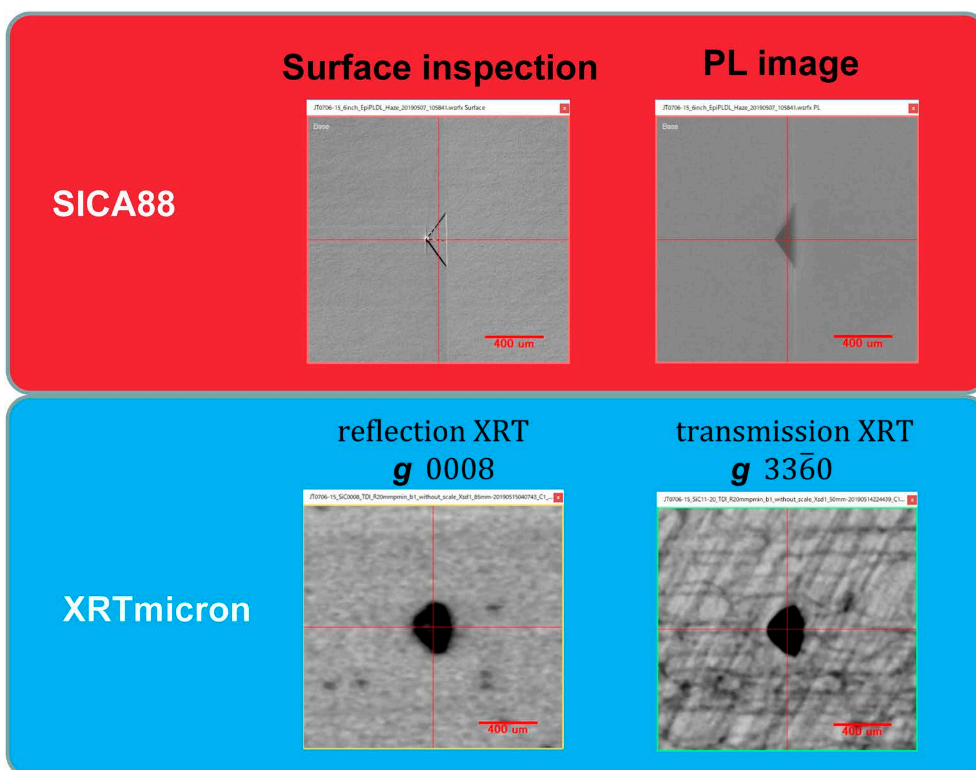

Fig. 13. XRT images by XRTmicron viewed on SICA analysis software platform.

display and analysis software of the SICA88 system to display XRT data obtained by the XRTmicron system.

An example is shown in Fig. 13. It is expected that the fabrication of devices with higher efficiency will be greatly promoted by research through collaborative analyses of various characterization techniques via elucidation of the nature of inherent impacting defects in SiC enabling to manipulate these defects, like reduction of dislocations, or their conversion to electrically benign dislocations, and so on.

6. Summary

Examples of XRT characterization using XRTmicron system for modern functional crystals, such as sapphire substrates, SAM substrates, etc., were demonstrated, after the introduction of XRTmicron system features and the explanation of the $\boldsymbol{g}\cdot\boldsymbol{b}$ analysis technique. Single crystal substrates are an important platform for the

growth of various functional thin film materials that will enrich our lives. Scientific studies or industrial research into these materials are supported by characterization techniques. It is hoped that the XRTmicron system will assist these activities as a powerful and influential tool.

Acknowledgements

We would like to offer great thanks to Prof. Dr. Tsuguo Fukuda in Fukuda Crystal Laboratory Co. Ltd, for providing SAM substrate for XRT characterization.

References

(1) K. Omote: *Rigaku Journal (English version),* **29** (2013), No. 1, 1–8.
(2) *Rigaku Journal (English version),* **30** (2013), No. 1, 30–32.
(3) *Rigaku Journal (English version),* **32** (2016), No. 1, 33–35.
(4) C. S. Barrett: *Trans. AIME,* **161** (1945), 15–64.
(5) A. R. Lang: *Jour. Appl. Phys.,* **29** (1958), 597–598.
(6) B. K. Tanner: *X-ray Diffraction Topography, Oxford Pergammon,* (1976).
(7) for example, *Rigaku Journal (English version),* **31** (2014), No. 1, 7–16.
(8) D. L. Stephens and W.J. Alford: *J. Amer. Ceram. Soc.*, **47** (1962), 81–86.
(9) K. P. D. Lagerlöf, A.H. Heuer, J. Casting and J. P. Rivière: *J. Amer. Ceram. Soc.*, **77** (1994), 385–397.
(10) A. H. Heuer, K.P.D. Lagerlöf and J. Casting: *Phil. Mag.*, **78** (1998), 747–763.
(11) K. Inaba and K. Omote: *29th International Conference on Defects in Semiconductors* (2017), Tup-73.
(12) N. Kimizuka and T. Mohri: *J. Solid State Chem.,* **78** (1989), 98–107.
(13) T. Fukuda, T. Matsuoka and S. Suzuki: ICPSCG10, (Zakopane, Poland, Oct. 15–21, 2016).
(14) R. Simura, K. Sugiyama, A. Nakatsuka and T. Fukuda: *Jpn. J. Appl. Phys.,* **54** (2015), 075503.
(15) *Fukuda Crystal Laboratory* website (in Japanese). https://fxtal2002.com/technology/crystal1
(16) A. Tanaka, H. Matsuhata, N. Kawabata, D. Mori, K. Inoue, M. Ryo, T. Fujimoto, T. Tawara, M. Miyazato, M. Miyajima, K. Fukuda, A. Ohtsuki, T. Kato, H. Tsuchida, Y. Yonezawa and T. Kimoto: *Jour. Appl. Phys.,* **119** (2016), 095711-1-095711-9.
(17) *Lasertec Corp.* website. https://www.lasertec.co.jp/products/environment/sic/sica88.html
(18) *TPEC* website. https://www.tia-nano.jp/tpec/en/index.html
(19) M. Hasegawa and T. Ohno: *Jour. Appl. Phys.,* **110** (2011), 073507-1-073507-6.
(20) T. Isshiki and M. Hasegawa: *Mater. Sci. Forum,* **821–823** (2015), 307.